

RESEARCH ARTICLE

Photonic passbands induced by optical fractal effect in Cantor dielectric multilayers

Jianxia Liu¹, Jing Shen^{1*}, Dong Zhao¹, Pu Zhang^{2*}

1 School of Electrical and Information Engineering, Hubei University of Science and Technology, Xianning, China, **2** Research Center for the Development of Rural Education and Culture, Key Research Base of Humanities and Social Sciences in Hubei Province, Hubei University of Science and Technology, Xianning, China

* shenjing@hust.edu.cn(JS); zhangpu@hust.edu.cn (PZ)



OPEN ACCESS

Citation: Liu J, Shen J, Zhao D, Zhang P (2022) Photonic passbands induced by optical fractal effect in Cantor dielectric multilayers. PLoS ONE 17(8): e0268908. <https://doi.org/10.1371/journal.pone.0268908>

Editor: Muhammad Zubair, Information Technology University, PAKISTAN

Received: February 16, 2022

Accepted: May 11, 2022

Published: August 2, 2022

Copyright: © 2022 Liu et al. This is an open access article distributed under the terms of the [Creative Commons Attribution License](https://creativecommons.org/licenses/by/4.0/), which permits unrestricted use, distribution, and reproduction in any medium, provided the original author and source are credited.

Data Availability Statement: All relevant data are within the paper and its [Supporting Information](#) files.

Funding: This work was supported by the Science and Technology Plan Research Project of Hubei Education Department (B2019156); the Scientific Research Project of Hubei University of Science and Technology (BK2020171); Natural Science Foundation of Hubei Province of China (2021CFB418); and the Co-operative Education Reform Project Innovative Undertaking Together of the Education Ministry for China (201901033016).

Abstract

We investigate the splitting and incorporation of optical fractal states in one-dimensional photonic quasi-crystals. The aperiodic crystals which are composed of two different dielectrics submit to Cantor sequence. Defects in Cantor crystals can greatly enhance the localization of electric field, which induces the optical fractal effect. The number of optical fractal states increases exponentially with the generation number of Cantor sequence. Moreover, the optical fractal characteristics depend on the incident angle of light, of which the fractal states may split/incorporate by modulating the value of incident angle. This study could be utilized for band-pass filters and reflectors.

1. Introduction

Fractal concept was first introduced by Mandelbrot in 1967 [1]. Fractal is an universal phenomenon in nature and has covered a wide range of the modern science from geography to nonlinear dynamics [2–4]. A fractal can be constructed based on the incorporation of identical motifs that repeat on different size scales. In optics issue, fractal structures can be contributed by three types, namely perfectly periodic media, absolutely random media and quasi-periodic media, respectively [5–7]. Compared with the periodic photonic crystals, quasi-periodic photonic crystals have displayed many unique features and have the particular interest for scientists [8–11].

Cantor sets of dielectric isotropic layers are the typical model fractal structures. Cantor-like dielectric superlattices (DSLs) have been studied widely on the structural and physical properties since Cantor sets were defined by G. Cantor in 1883 [12]. In contrast with Thue-Morse- and Fibonacci-like superlattices, the unit cell thickness of Cantor type DSLs increases with the sequence step [13–15]. Many excellent features and behaviors were concerned by the scientists around the world in the past twenty years. Such as, the self-similarity behavior of the reflectance and transmission spectra of Cantor type DSLs [16], the effective index and third order nonlinear susceptibilities of Cantor structures [17], the scaling properties of optical Cantor filters [18], the second harmonic generation and the third harmonic generation of Cantor type DSLs [19], the photonic bandgap behavior and the optical windows presence of one-dimensional

Competing interests: The authors have declared that no competing interests exist.

triadic Cantor quasi-periodic structures [20], the tunable multichannel filter property based on the use of periodic Cantor dielectric multilayers [21], the second harmonic generation in Cantor like metamaterial photonic superlattices [22], the unidirectional absorption properties of the defective asymmetric Cantor photonic crystals [23], the self-similarity feature of complex quasi-periodic Fibonacci and Cantor photonic crystals [24].

In this work, the studies only focus on the Cantor dielectric multilayers that are quasi-periodic (or aperiodic) photonic crystals composed of two different dielectrics Si and SiO₂. The discussions are summarized as follows: (a) Transmission spectra and the distributions of the electrical field are analyzed using one-dimensional transfer matrix method. (b) Optical fractal effect is analyzed and discussed. The formula to compute the number of optical fractal states is established. The results show that it is matched very well between the formula calculation and the numerical simulation. (c) Optical fractal effect is analyzed with the change of incident angle of light. We find that the optical fractal states may split/incorporate by modulating the value of incident angle. The pass-bands are produced with the incorporation of the optical fractal states. It is a candidate to be applied in band-pass filters.

2. Cantor multilayers

In this study, an one-dimensional photonic quasi-crystal is proposed. It is an aperiodic crystal which is composed of two different dielectrics and submits to Cantor sequence law [25]. Each of the Cantor dielectric multilayers is characterized by a fundamental parameter N , viz. the generation number N , where N is an integer of 0, 1, 2, 3 in turn. There is only one layer for $N = 0$. With the increase of the generation number N , the number of the crystal layers will increase rapidly with 3^N law. For instance, the number of the crystal layers is 3, 9 and 27 for the generation number $N = 1, 2$ and 3, respectively. Fig 1 gives the diagram of the Cantor dielectric multilayers for different generation number N . The red layers represent the higher index dielectric Si and the green layers represent lower index dielectric SiO₂. The refractive indices of the two dielectrics Si and SiO₂ are $n_a = 3.53$ and $n_b = 1.46$, respectively [26, 27]. The thicknesses of dielectric slabs are 1/4 optical wavelengths, viz. $d_a = \lambda_0/4/n_a = 0.1098 \mu\text{m}$ (denoted in red) and $d_b = \lambda_0/4/n_b = 0.2654 \mu\text{m}$ (denoted in green), where $\lambda_0 = 1.55 \mu\text{m}$ is the central wavelength. The substrate surrounding of the aperiodic system is air and its refractive index is set as 1.

The transfer matrix method [28] is used to investigate the transmission spectra of light in the Cantor dielectric multilayers. The path diagram of the optical wave transmitting in the Cantor dielectric multilayers is shown in Fig 2. The alphabet θ_i is the incident angle of light from the air to the multilayer medium and θ_o is the output angle of light from the multilayers to the external environment. The horizontal direction to the right is the positive direction of the Z-axis and the vertical up direction is the positive direction of the Y-axis. The transfer matrix of each layer is written in the following form of

$$T_j = \begin{bmatrix} \cos \delta_j & \frac{i}{\eta_j} \sin \delta_j \\ i\eta_j \sin \delta_j & \cos \delta_j \end{bmatrix}. \quad (1)$$

shift of light δ_j is calculated using the following formula

$$\delta_j = \frac{2\pi}{\lambda} n_j d_j \cos \theta_j, \tag{3}$$

where η_j is the effective optical admittance of the j -th layer and is calculated by

$$\eta_j = \eta_0 n_j \cos \theta_j, \tag{4}$$

where $\eta_0 = \sqrt{\frac{\epsilon_0}{\mu_0}}$ is the optical impedance admittance in vacuum, n_j is the refractive index of the j -th layer and $d_j = \lambda_0/4n_j$ is the j -th layer thickness, λ_0 is the reference wavelength of light and λ is the working wavelength of light.

The transmission coefficient of electric field is calculated by

$$t = \frac{2\eta_j}{A\eta_j + B\eta_j\eta_0 + C + D\eta_0}. \tag{5}$$

The intensity of the output light is obtained by

$$I_o = I_i |t|^2 = I_i T, \tag{6}$$

where I_i is the input intensity of light and T is named as the transmittance of optical intensity.

3. Optical fractal effect

Optical fractal is a typical effect in the quasi-periodicity photonic crystals. The resonant states expand exponentially as the generation number N of photonic crystals increases. We here demonstrate the transmission spectra of lights in the Cantor dielectric multilayers for different values of N .

For a transverse magnetic (TM) wave, as it impinges on the Cantor photonic crystal from the left, Fig 3A describes the transmission spectrum of light for $N = 1$. The horizontal coordinate $(\omega - \omega_0)/\omega_{\text{gap}}$ is the normalized frequency of the incidence light waves, where $\omega = 2\pi c/\lambda$, $\omega_0 = 2\pi c/\lambda_0$ and $\omega_{\text{gap}} = 4\omega_0 \arcsin \left| \frac{[\text{Re}(n_H) - \text{Re}(n_L)]}{[\text{Re}(n_H) + \text{Re}(n_L)]} \right|^2 / \pi$ are respectively called as the incident angular frequency of light, the central angular frequency and photonic bandgap. c is the vacuum velocity of light. We here borrow the concept of photonic bandgap in periodic photonic crystals and give four spectral periods for each generation number N . One period length has been noted in the area between two blue dotted lines. Four periods have been noted in the area between green dotted lines E and F. There are 3 resonance peaks in one spectral period and 12 resonance peaks in four spectral periods for $N = 1$.

For $N = 2$, the resonant states increase to 9 in a period unit of transmission spectrum. The total quantity is as high as 36 in four period units as shown in Fig 3B. In the same way, 27 resonance peaks can be counted in one spectral period in Fig 3C and the number of the valid resonance peaks in four spectral periods is 108. Moreover, some peaks are produced by splitting and some others are new generating. Obviously, the optical fractal effect of the Cantor dielectric multilayers is observed with the increase of the generation number N .

Resonance frequencies versus different generation number N for two spectral periods are given in Fig 4. The number of the resonance peaks for $N = 1, 2$ and 3 is counted respectively. The number of the resonance peaks increases exponentially with the increase of the generation number N . Because each resonant peak represents an optical fractal state, the optical fractal states increases proportionally with N as well. According to Fig 4, the number of the optical fractal states is counted for the generation number $N = 1, 2$ and 3 , respectively. Because the number of the optical fractal states is large for the generation number $N = 4$, it is not clear to

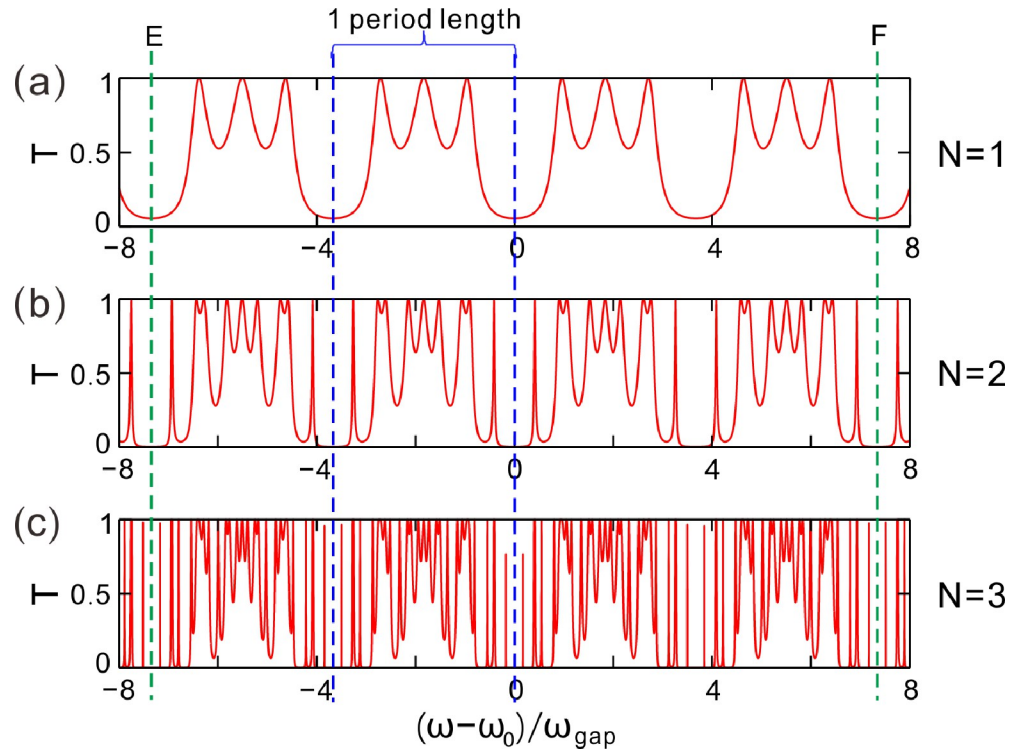


Fig 3. (a-c) Transmittance varying with the frequencies of the incident light wave for the generation number $N = 1, 2$ and 3 , respectively. Here, incident angle of light $\theta_i = 0^\circ$.

<https://doi.org/10.1371/journal.pone.0268908.g003>

be demonstrated. For showing obviously the number of the optical fractal states, the area I is amplified and the details are displayed in subgraph II.

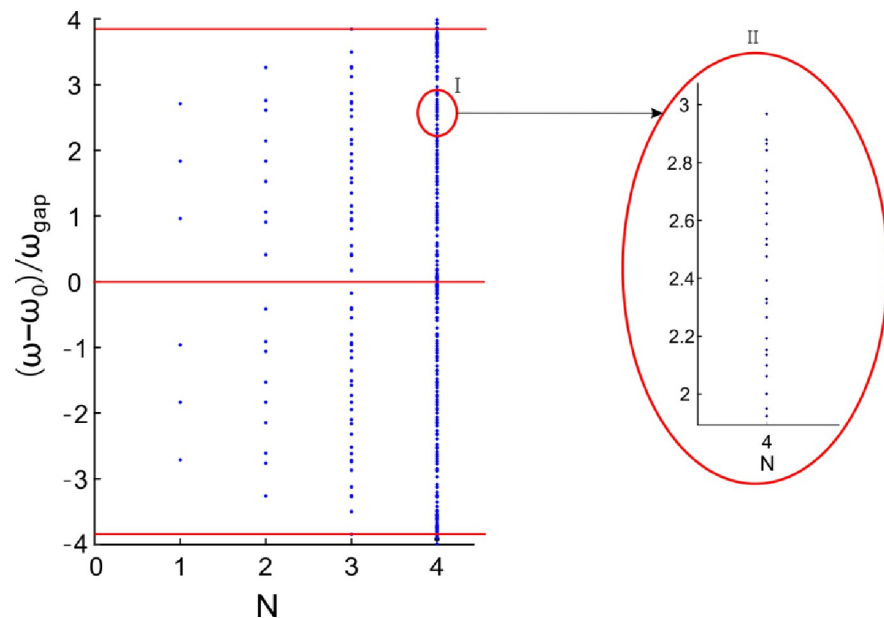


Fig 4. Frequencies of resonance peaks versus the generation number $N = 1, 2, 3$ and 4 , respectively.

<https://doi.org/10.1371/journal.pone.0268908.g004>

According to the above discussion, the optical fractal effect in the Cantor dielectric multilayers is expressed as sequential splitting. Namely, a spectral line is splitting into multiplets. The reason for the sequential splitting can be understood from the point of view of self-similarity of the Cantor dielectric multilayers regarded in terms of coupled cavities. At the same time, some new spectral lines also generate in forbidden bands. The number of the sequential splitting and the new generated spectral lines are respectively expressed by

$$P_{new} = \frac{G - 1}{2}, \quad (7)$$

$$P_{splitting} = \frac{G + 1}{2}. \quad (8)$$

The total number of the spectral lines is computed by

$$P_{total} = G^N, \quad (9)$$

where G is the generator and N is the generation number. In this work, the generator G is set to 3. According to the Eq (9), the total number of the splitting spectral lines is 3, 9, 27, and 81 for the generator $G = 3$ and the generation number $N = 1, 2, 3$ and 4, respectively. The quantitative relationship between the total spectral lines and the generation number N has been showed in Table 1. Compared with the features in Figs 3 and 4, it is matched very well between the theoretical calculation and the numerical simulation in Table 1.

For observing the electric field distributions of optical fractal states in the Cantor dielectric multilayers, two spectral periods of transmission for the generation number $N = 2$ are displayed in Fig 5A. There are 18 resonance peaks marked, *viz.* 18 optical fractal states. Three optical fractal states are arbitrarily selected, *viz.* the 13-th, 14-th, and 15-th peak, and their electric field distributions are simulated as well. The corresponding wavelengths are the values of $\lambda_{13,14,15} = 0.7149, 0.7759$ and $0.8461 \mu\text{m}$, respectively.

The finite difference time domain (FDTD) is taken to simulate the electric field distributions. Fig 5B gives the electric field distribution for $\lambda_1 = 0.7149 \mu\text{m}$. The mode field power is mainly distributed in the low index defects and the intensity decays from the center to both the left and right sides exponentially. The electric fields are stronger in the three center defects than these of the two terminal defects in the dielectric multilayers. At the same time, the electric field distribution shows a good central symmetry. Here the optical loss in the dielectrics is not considered since the loss of dielectrics is low and it does not impress optical fractal effect severely. The transmission peaks are almost coincident for the case containing loss in dielectrics and the case without loss. The corresponding electric field distribution of λ_1 is more concentrated than that of λ_2 and λ_3 .

Fig 5C gives the electric field distribution for $\lambda_2 = 0.7759 \mu\text{m}$. The mode field is distributed in the low index defects and decays from the center to both the left and right sides. The electric field distribution shows a good central symmetry as well. However, the corresponding electric field distribution of λ_2 is quite different from that of λ_1 . The maximum power of electric field

Table 1. Quantitative relationship between the total spectral lines and the generation number N .

N	P_{total}
1	3
2	9
3	27
4	81

<https://doi.org/10.1371/journal.pone.0268908.t001>

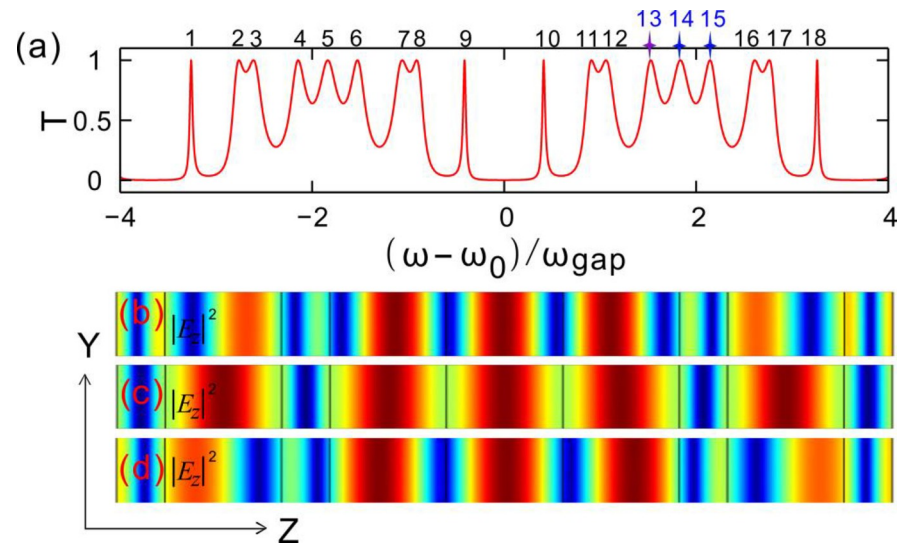


Fig 5. (a) Transmittance varying with the frequencies of incident light wave for the generation number $N = 2$. (b-d) Electric field distributions of the 13-th, 14-th and 15-th optical fractal state, respectively. The incident angle of light is $\theta_i = 0^\circ$.

<https://doi.org/10.1371/journal.pone.0268908.g005>

locates in the three middle defects and the two terminal defects of the dielectric multilayers. There is not an almost forbidden band in the three middle defects for the electric field transmission. Therefore, it is easy to produce a passband with the central wavelength of λ_2 .

Fig 5D gives the electric field distribution for $\lambda_3 = 0.8461 \mu\text{m}$. The mode field power is mainly distributed in the low index defects and decays from the center to both the left and right sides. The electric fields are stronger in the three center defects than that of the two terminal defects of the dielectric multilayers. The electric field distribution shows a good center symmetry as well. The distribution is similar with that of λ_1 . However, comparing with the electric field distribution of λ_1 , the band width of either pass-band or forbidden band is wider than that of λ_1 . In addition, the electric field intensity reverses between the wavelength λ_1 and the wavelength λ_2 .

Defects in photonic crystals can greatly localize the electric field [29]. Defects in Cantor crystals can tremendously enhance the localization of electric field as well, which results in the optical fractal effect in aperiodic structures. The periodic photonic crystals support the photonic bandgap, while for the defective photonic crystals, the defect resonance modes, *viz.* transmitted modes, arise in the bandgap. The Cantor photonic crystals are aperiodic and many defects exist in the systems, so it approves a series of resonant transmitted states in the spectra. The resonant transmitted states split as the generation number increases. Consequently, the defect resonance modes in aperiodic photonic crystals are called the optical fractal states. The passband results from the incorporation of optical fractal states by modulating the incident angle. Therefore, the optical fractal effect is absent in the periodic photonic crystals. Otherwise, there are passbands on both sides of the bandgap as well, and the transmittance in this mentioned passband fluctuates as the frequency of light wave changes, of which the corresponding transmission peak is the standing wave resonance.

4. Fractal states incorporation and splitting

The spectral properties of the dielectric multilayers are analyzed through changing the incident angle of light. Two spectral periods on different incident angles of light are shown in Fig 6. The generation number is $N = 2$. Fig 6A shows the spectrum for the incident angle of light $\theta_i =$

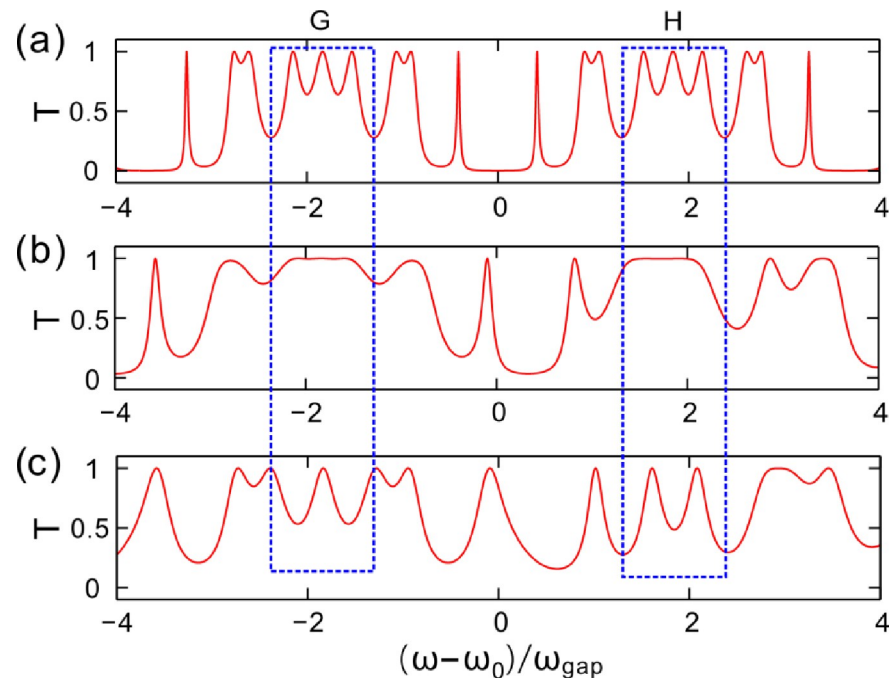


Fig 6. (a-c) Transmittance varying with the frequency of the incident light wave for the incident angle of 0° , 65° and 80° , respectively. Here, the generation number is $N = 2$.

<https://doi.org/10.1371/journal.pone.0268908.g006>

0° . The spectral distribution is the same with that in Fig 5A and there are 18 optical fractal states in the transmission spectrum of light.

Fig 6B shows the spectrum for the incident angle of light $\theta_i = 65^\circ$. The spectrum is quite different from that of the incident angle $\theta_i = 0^\circ$. The number of the optical fractal states changes from 18 to 9. The number has been reduced by a half. The two pass bands appear and are marked in two blue rectangles G and H. In Fig 6A and 6B, the incorporation of the optical fractal states is resulted in the Cantor dielectric multilayers with the change of the incident angle of light from 0° to 65° . The 4-th, the 5-th and the 6-th optical fractal state in Fig 6A incorporate into the third optical fractal state in Fig 6B (Denoting the optical fractal states from the left to right). The 13-th, the 14-th and the 15-th optical fractal state in Fig 6A incorporate into the seventh optical fractal state in Fig 6B.

For the incident angle of light $\theta_i = 80^\circ$, the spectrum of light is showed in Fig 6C. The change of the spectrum is obvious. Comparing with Fig 6B and 6C shows that some optical fractal states split and two pass bands disappear. The band optical fractal states confined in the areas of the blue rectangle G in Fig 6B do not split as the incident angle increases, but it gradually forms an optical fractal state with a narrow bandwidth. In addition, the pass band of transmission spectrum in the right rectangular H in Fig 6B splits into two optical fractal states as the incident angle is $\theta_i = 80^\circ$.

The Cantor photonic crystals investigated here are passive, of which the material loss is weak and has been ignored in the whole simulation process to highlight the optical fractal effect, so the systems are not non-Hermitian. Especially, the Cantor photonic crystals are aperiodic and the defects increase with the increase of the generation number of sequence, which demonstrates more resonant states induced in the transmission spectra and the states split by increasing the generation number, *viz.* optical fractal effect. Otherwise, the resonance of each fractal state decreases and the width of resonant peak widens as the incident angle increases,

which results in two adjacent resonant peaks overlapping each other and connecting together to form a passband, while for the non-Hermitian system, the eigenvectors and eigenvalues coalesce at the exceptional point (EP) [30]. Therefore, the merging of optical fractal states in aperiodic structures differs from the coalescence of the eigenvectors and eigenvalues at EP in non-Hermitian systems. Otherwise, non-Hermitian systems have been intensively investigated to be utilized for electric field localization, solitons, topological edge states, topological insulators and chiral mode transfers [31–38].

Therefore, the optical fractal states incorporate as the increase of the incident angle from the incident angle $\theta_i = 0^\circ$. The wide bandpass is obtained as the incident angle of light increases to $\theta_i = 65^\circ$. As the incident angle of light continues to increase to $\theta_i = 80^\circ$, the splitting of the optical fractal states is observed again. However, the splitting of the optical fractal states cannot be recovered into the beginning profile. Some new optical fractal states are formed. Through selecting suited incident angle of light, the optical fractal states of the spectra are modulated. The characteristics could be utilized to design the band-pass filters and reflectors.

For presenting more clearly the incorporation and the splitting of the optical fractal states. The transmittance and the reflectance versus the incident angle of light and the normalized frequency are given. Fig 7A presents the transmittance as the change of the incident angle of light and the normalized frequencies. The incorporation of the optical fractal states is observed obviously as the incident angle of light increases. Two wide passbands appear in the areas marked in two green ellipses III and IV, respectively. The two wide passbands produce as the incident angle of light is $\theta_i = 65^\circ$. The widths of the two passbands become narrower as one keeps increasing the incident angle of light. The splitting appears for the incident angle of light $\theta_i = 80^\circ$.

Fig 7B presents the reflectance as the incident angle of light and the normalized frequency increases. The intensity distributions are the opposite of that of the transmittance in Fig 7A. It is well known that the maximum of transmittance corresponds to the minimum of reflectance. Obviously, it is matched very well between the simulation results and the theory. Six good reflective bands are observed and are marked as S1, S2, S3, S4, S5, and S6, respectively. Using the properties of the reflectance of the Cantor dielectric multilayers, the multi-wavelengths reflectors can be designed as well.

The Cantor photonic crystals here are passive, which dominates the sum of transmittance and reflectance $T + R \leq 1$. To demonstrate this property more clearly, we give the transmission and reflection spectra changing with the normalized frequency for a fixed incident angle $\theta_i = 65^\circ$ as shown in Fig 7C. One can see that, for each given incident frequency of light wave, the value satisfies the formula $T(\omega) + R(\omega) \leq 1$. Changing the incident angle, the above expression is true as well.

In fact, both transverse magnetic and transverse electric polarized waves can be used to achieve optical fractal effect and photonic passbands in Cantor photonic crystals here. Avoiding repetition, we here only give the spectra of light for the transverse magnetic waves.

5. Conclusions

In conclusion, the splitting and incorporation of optical fractal states in one-dimensional photonic quasi-crystals have been studied. The aperiodic crystals which are composed of two different dielectrics submit to the Cantor sequence law. Defects located in the Cantor multilayers can restrict greatly the power of the electric fields, which approves to induce an optical fractal effect. Scalability and sequential splitting of the spectra are observed as well. Furthermore, the optical fractal states increase exponentially with the increase of the sequence number. The number of the optical fractal states is obtained by the theoretical calculation and the numerical simulation. The results show that it is matched very well between the two simulating methods. Moreover, the optical fractal effect

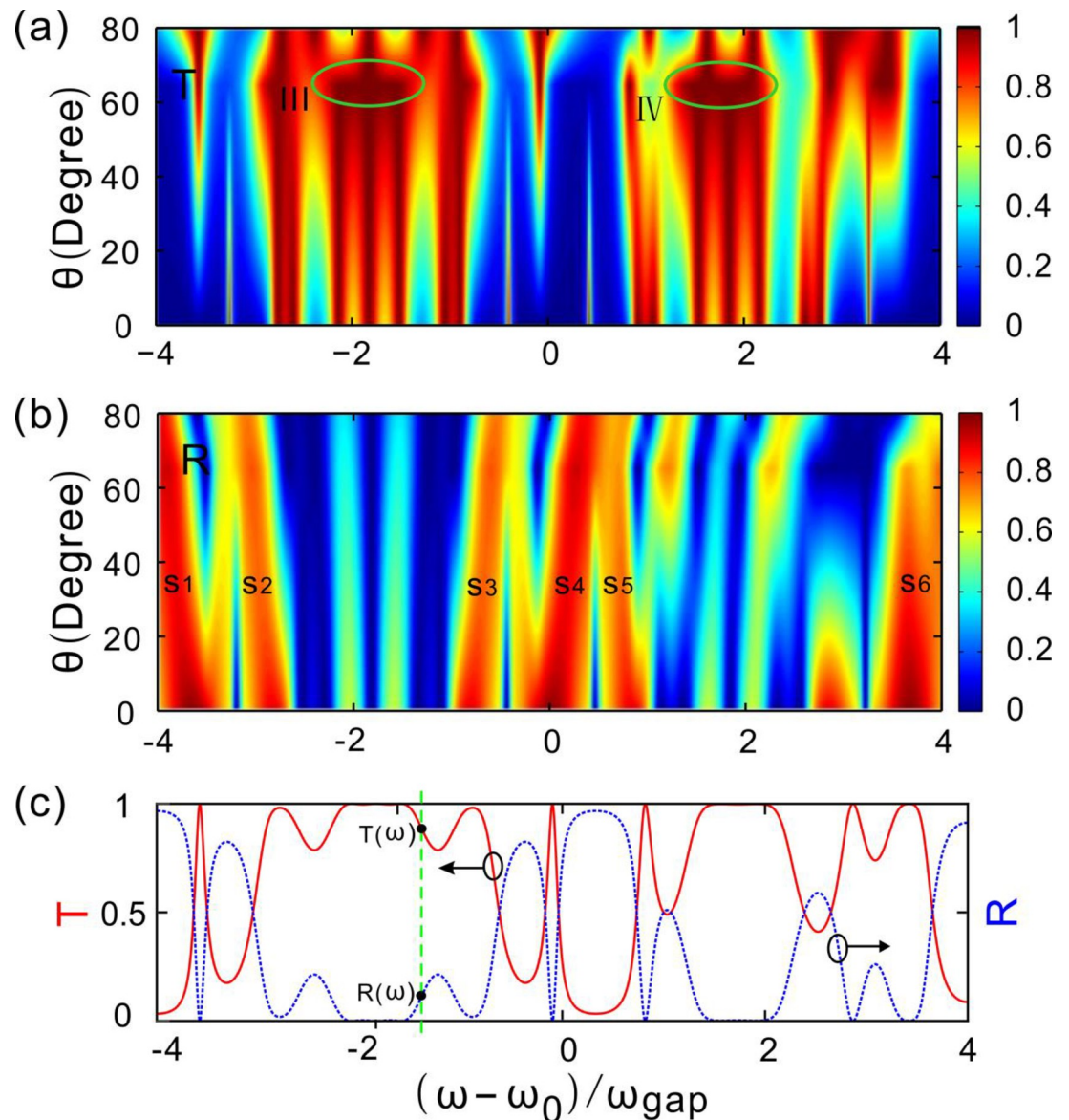


Fig 7. (a, b) Transmittance and reflectance versus the incident angle of light and the normalized frequency, respectively. (c) Transmission spectrum and the reflectance spectra for incident angle $\theta_i = 65^\circ$.

<https://doi.org/10.1371/journal.pone.0268908.g007>

depends on the incident angle of light, of which the optical fractal states can split/incorporate by modulating the incident angle of light. The optical fractal states incorporate as the incident angle of light changes. Wide passbands appear at the incident angle of light $\theta_i = 65^\circ$. If one keeps increasing of the incident angle of light, the splitting of the optical fractal states appears. However, the splitting cannot recover the optical fractal states into the beginning states and some new optical fractal states are formed. This study could be utilized for band-pass filters and reflectors.

Supporting information

S1 Dataset.

(RAR)

Author Contributions

Conceptualization: Jianxia Liu.

Data curation: Jing Shen.

Formal analysis: Jianxia Liu, Jing Shen, Pu Zhang.

Funding acquisition: Jianxia Liu, Dong Zhao.

Investigation: Jianxia Liu, Pu Zhang.

Project administration: Jing Shen, Dong Zhao, Pu Zhang.

Software: Jianxia Liu, Dong Zhao.

Supervision: Jing Shen, Pu Zhang.

Validation: Pu Zhang.

Visualization: Jing Shen.

Writing – original draft: Jianxia Liu.

Writing – review & editing: Jianxia Liu, Jing Shen, Dong Zhao, Pu Zhang.

References

1. Mandelbrot B. How long is the coast of Britain? Statistical self-similarity and fractional dimension. *Science*. 1967; 156(3775): 636–638. <https://www.science.org/doi/10.1126/science.156.3775.636> PMID: 17837158
2. Encalada-Abarca L.; Ferreira CC; Rocha J. Measuring tourism intensification in urban destinations: an approach based on fractal analysis. *Journal of Travel Research*. 2022; 61(2): 394–413. <https://doi.org/10.1177/0047287520987627>
3. Bounoua W; Bakdi A. Fault detection and diagnosis of nonlinear dynamical processes through correlation dimension and fractal analysis based dynamic kernel PCA. *Chemical Engineering Science*. 2021; 229: 116099. <https://doi.org/10.1016/j.ces.2020.116099>
4. Wang KL; Wei CF. A powerful and simple frequency formula to nonlinear fractal oscillators. *Journal of Low Frequency Noise, Vibration and Active Control*. 2021; 40(3): 1373–1379. <https://doi.org/10.1177/1461348420947832>
5. Chigrin DN; Lavrinenko AV; Yarotsky DA; Gaponenko SV. All-dielectric one-dimensional periodic structures for total omnidirectional reflection and partial spontaneous emission control. *Journal of Lightwave Technology*. 1999; 17(11): 2018. <https://ieeexplore.ieee.org/document/802989>
6. Zhang X; Ostoja-Starzewski M. Impact force and moment problems on random mass density fields with fractal and Hurst effects. *Philosophical Transactions of the Royal Society A*. 2020; 378(2172): 20190591. <https://doi.org/10.1098/rsta.2019.0591> PMID: 32389090
7. Elsayed HA; Abadla MM. Transmission investigation of one-dimensional Fibonacci-based quasi-periodic photonic crystals including nanocomposite material and plasma. *Physical Scripta*. 2020; 95: 035504. <https://iopscience.iop.org/article/10.1088/1402-4896/ab4c68>
8. Jun W. TPP-assisted multi-band absorption enhancement in graphene based on Fibonacci quasiperiodic photonic crystal. *Results in Physics*. 2022; 33: 105210. <https://doi.org/10.1016/j.rinp.2022.105210>
9. Osswa S; Jihene Z; Mounir K. Tunable filter properties in 1D linear graded magnetized cold plasma photonic crystals based on Octonacci quasi-periodic structure. *Photonics and Nanostructures*. 2020; 38: 100744. <https://doi.org/10.1016/j.photonics.2019.100744>
10. Imanian H; Noori M; Abbasiyan A. Highly efficient gas sensor based on quasi-periodic phononic crystals. *Sensor and Actuators B: Chemical*. 2021; 345: 130418. <https://doi.org/10.1016/j.snb.2021.130418>
11. Guo S; Hu C; Zhang H. Analysis of the features of a multifunctional device based on the regulation of the magnetic field in one-dimensional photonic crystals containing only plasma with a novel quasi-periodic structure. *Journal of the Optical Society of America B*. 2020; 37(7): 1996–2005.
12. Cantor G. Ueber unendliche, lineare Punktmanichfaltigkeiten. *Mathematische Annalen*. 1883; 23: 453–488. <https://doi.org/10.1007/BF01446598>

13. Gómez FR; Porrás-Montenegro N; Jr., ONO; Mejía-Salazar JR. Second harmonic generation in the plasmonpolariton gap of quasiperiodic metamaterial photonic superlattices. *Physical Review B*. 2018; 98(7): 075406. <https://journals.aps.org/prb/abstract/10.1103/PhysRevB.98.075406>
14. Omar AA. Design of ultrawideband coplanar waveguide-fed Koch-fractal triangular antenna. *International Journal of RF and Microwave Comput-Aided Engineering*. 2013; 23(2): 200–207. <https://onlinelibrary.wiley.com/doi/10.1002/mmce.20665>
15. Bellido EP; Bernasconi GD; Rossouw D; Butet J; Martin OJF; Botton GA. Self-similarity of plasmon edge modes on Koch fractal antennas. *ACS Nano*. 2017; 11(11): 11240–11249. <https://pubs.acs.org/doi/10.1021/acsnano.7b05554> PMID: 29083865
16. Vasconcelos MS; Albuquerque EL. Plasmon polaritons and optical spectra of a superlattice of Cantor type. *Physica B*. 1996; 222: 113–122. <https://doi.org/10.1021/acsnano.7b05554>
17. Sibilia C; Tropea F; Bertolotti M. Enhanced nonlinear optical response of Cantor-like and Fibonacci-like quasiperiodic structures. *Journal of Modern Optics*. 1998; 45(11): 2255–2267. <https://doi.org/10.1080/09500349808231237>
18. Lavrinenko AV; Zhukovsky SV; Sandomirski KS; Gaponenko SV. Propagation of classical waves in nonperiodic media: scaling properties of an optical Cantor filter. *Physical Review E*. 2002; 65(3): 036621. <https://doi.org/10.1103/PhysRevE.65.036621> PMID: 11909299
19. Cai X. Optical harmonic generation in the Cantor-type dielectric superlattice. *Journal of Optics A: Pure and Applied Optics*. 2003; 5(4): 323–327. <https://iopscience.iop.org/article/10.1088/1464-4258/5/4/303>
20. Sahel S; Amri R; Bouaziz L; Gamra D; Lejeune M; Benlahsen M; et al. Optical filters using Cantor quasiperiodic one dimensional photonic crystal based on Si/SiO₂. *Superlattices and Microstructures*. 2016; 97: 429–438. <https://doi.org/10.1016/j.spmi.2016.07.007>
21. King TC; Wu CJ. Design of multichannel filters based on the use of periodic Cantor dielectric multilayers. *Applied Optics*. 2014; 53(29): 6749–6755. <https://doi.org/10.1364/AO.53.006749> PMID: 25322378
22. Gómez FR; Porrás-Montenegro N; Jr. ONO; Mejía-Salazar JR. Giant second-harmonic generation in Cantor-like metamaterial photonic superlattices. *ACS Omega*. 2018; 3(12): 17922–17927. <https://doi.org/10.1021/acsomega.8b02837> PMID: 31458384
23. King TC; Dong YM. Unidirectional absorption properties in a defective semiconductor-dielectric asymmetric triadic Cantor photonic crystal. *Physica E*. 2019; 108: 135–138. <https://doi.org/10.1016/j.physe.2018.12.006>
24. Augustyniak A; Zdanowicz M; Osuch T. Self-similarity properties of complex quasi-periodic Fibonacci and Cantor photonic crystals. *Photonics*. 2021; 8(12): 558. <https://doi.org/10.3390/photonics8120558>
25. Feder J. *Fractals*. Springer Science & Business Media. New York. 2013.
26. Ni H; Wang J; Wu A. Optical bistability in aperiodic multilayer composed of graphene and Thue-Morse lattices. *Optik*. 2021; 242: 167163. <https://doi.org/10.1016/j.ijleo.2021.167163>
27. Wang J; Xu F; Liu F; Zhao D. Optical bistable and multistable phenomena in aperiodic multilayer structures with graphene. *Optical Materials*. 2021; 119: 111395. <https://doi.org/10.1016/j.optmat.2021.111395>
28. Li J; Zhu X; Shen C; Xiuyuan Peng; Cummer SA. Transfer matrix method for the analysis of space-time-modulated media and systems. *Physical Review B*. 2019; 100(14): 144311. <https://doi.org/10.1103/PhysRevB.100.144311>
29. Guo Z; Jiang H; Chen H. Zero-index and hyperbolic metacavities: fundamentals and applications. *Journal of Physics D: Applied Physics*. 2022; 55: 083001. <https://iopscience.iop.org/article/10.1088/1361-6463/ac2e89>
30. Guo Z; Zhang T; Song J; Jiang HT; Chen H. Sensitivity of topological edge states in a non-Hermitian dimer chain. *Photonics Research*. 2021; 9: 574–582. <https://doi.org/10.48550/arXiv.2007.04409>
31. Li S; Wang S; Chen S; Wu Y; Ke S; Wang B; et al. Subspace-induced Dirac point and nondissipative wave dynamics in a non-Hermitian optical lattice. *Physical Review A*. 2022; 105: 033512.
32. Zhao Y; Lei YB; Xu YX; Xu SL; Triki H; Biswas A; et al. Vector spatiotemporal solitons and their memory features in cold Rydberg gases. *Chinese Physics Letters*. 2022; 39: 034202. <https://iopscience.iop.org/article/10.1088/0256-307X/39/3/034202>
33. Ke S; Zhao D; Fu J; Liao Q; Wang B; Lu P. Topological edge modes in non-Hermitian photonic Aharonov-Bohm cages. *IEEE Journal on Selected Topics in Quantum Electronics*. 2020; 26(6): 4401008. <https://ieeexplore.ieee.org/document/9146199>
34. Xiang S; Wu Y; Wang F; Lin Z; Hong Z; Ke S. Constant intensity discrete diffraction in anti-PT-symmetric electric circuits. *Results in Physics*. 2021; 27: 104491. <https://doi.org/10.1016/j.rinp.2021.104491>

35. Lin Z; Ding L; Ke S; Li X. Steering non-Hermitian skin modes by synthetic gauge fields in optical ring resonators. *Optics Letters*. 2021; 46(15): 3512–3515. <https://doi.org/10.1364/OL.431904> PMID: [34329212](https://pubmed.ncbi.nlm.nih.gov/34329212/)
36. Ding L; Lin Z; Ke S; Wang B; Lu P. Non-Hermitian flat bands in rhombic microring resonator arrays. *Optics Express*. 2021; 29(15): 24373–24386. <https://doi.org/10.1364/OE.431038> PMID: [34614684](https://pubmed.ncbi.nlm.nih.gov/34614684/)
37. Lin Z; Ke S; Zhu X; Li X. Square-root non-Bloch topological insulators in non-Hermitian ring resonators. *Optics Express*. 2021; 29(3): 8462–8476. <https://doi.org/10.1364/OE.419852> PMID: [33820293](https://pubmed.ncbi.nlm.nih.gov/33820293/)
38. Liu Q; Liu J; Zhao D; Wang B. On-chip experiment for chiral mode transfer without enclosing an exceptional point. *Physical Review A*. 2021; 103: 023531. <https://journals.aps.org/pr/abstract/10.1103/PhysRevA.103.023531>